













Cite this: *Biomater. Sci.*, 2020, **8**, 6261

# Augmented peripheral nerve regeneration through elastic nerve guidance conduits prepared using a porous PLCL membrane with a 3D printed collagen hydrogel†

Jin Yoo,  ‡<sup>a</sup> Ji Hun Park,  ‡<sup>b</sup> Young Woo Kwon,  ‡<sup>c</sup> Justin J. Chung,  In Cheul Choi,  <sup>d</sup> Jae Joon Nam,  <sup>d</sup> Hyun Su Lee,  <sup>e</sup> Eun Young Jeon,  <sup>a</sup> Kangwon Lee,  <sup>e</sup> Soo Hyun Kim,  <sup>a,f</sup> Youngmee Jung  <sup>\*a,g</sup> and Jong Woong Park  <sup>\*d</sup>

Peripheral nerve injury results in significant sensory and motor functional deficits. Although direct neurorrhaphy in the early phase may reduce its devastating effects, direct end-to-end neurorrhaphy is sometimes impossible owing to a defect at the injured site of the nerve. Autogenous nerve graft is a primary consideration for peripheral nerve defects; however, significant morbidity of the donor site is inevitable. Recently, the treatment using engineered synthetic nerve conduits has been regarded as a promising strategy to promote the regeneration of peripheral nerve defects. In this study, we developed longitudinally oriented collagen hydrogel-grafted elastic nerve guidance conduits (NGC) to reconstruct sciatic nerve defects. An elastic NGC was prepared by using poly(lactide-co-caprolactone) (PLCL), and electrospun PLCL was adopted to fabricate nanoporous structures with appropriate permeability for nerve regeneration. Oriented collagen hydrogels were prepared by the 3D printing method to achieve a microscale hydrogel pattern. Based on sciatic nerve injury models in rats, we confirmed the beneficial effects of the NGC with 3D printed collagen hydrogel on axonal regeneration and remyelination along with superior functional recovery in comparison with the NGC filled with the bulk collagen hydrogel. It is believed that the aligned collagen hydrogels provide a preferable environment for nerve regeneration, functioning as an oriented guidance path. In conclusion, the PLCL nerve guide conduit containing a 3D printed aligned collagen hydrogel can be useful for peripheral nerve regeneration.

Received 21st May 2020,  
Accepted 11th September 2020  
DOI: 10.1039/d0bm00847h  
rsc.li/biomaterials-science

## 1. Introduction

Peripheral nerve injury results in significant sensory and motor functional deficits. Although direct neurorrhaphy in the early phase may reduce its devastating effects, direct end-to-

end neurorrhaphy is sometimes impossible owing to a defect at the injured site of the nerve.<sup>1</sup> Autogenous nerve graft is a primary consideration for peripheral nerve defects. However, significant morbidity of the donor site is inevitable. Furthermore, several limitations such as mismatch of size and length between the donor and recipient nerves remain a hurdle in peripheral nerve reconstruction.<sup>2</sup> To overcome these issues associated with the autogenous nerve grafts, nerve graft substitutes have been tested using the autogenous vessel, muscle, decellularized allograft, and synthetic conduits. Among several substitution strategies, the artificial nerve guidance conduit (NGC) has been identified as a good alternative for autografts, as it can overcome differences in length and size between the donor and recipient nerves.<sup>3</sup> Thus, over the last decade, intensive research efforts have been devoted to fabricating NGCs with various types of materials, structures, compositions *etc.*<sup>4</sup> However, the inferior regeneration potential of artificial NGCs remains a concern.

To achieve ideal NGCs, their design and fabrication require the consideration of several factors, *i.e.*, material biocompat-

<sup>a</sup>Center for Biomaterials, Biomedical Research Institute, Korea Institute of Science and Technology (KIST), Seoul, Republic of Korea. E-mail: winnie97@kist.re.kr

<sup>b</sup>Department of Orthopedic Surgery, Korea Guro Hospital, Seoul, Republic of Korea

<sup>c</sup>Department of Orthopedic Surgery, Eulji Medical Center, Seoul, Republic of Korea

<sup>d</sup>Department of Orthopedic Surgery, Korea University Anam Hospital, Seoul, Republic of Korea. E-mail: ospark@korea.ac.kr

<sup>e</sup>Program in Nanoscience and Technology, Graduate School of Convergence Science and Technology, Seoul National University, Seoul, Republic of Korea

<sup>f</sup>KU-KIST Graduate School of Converging Science and Technology, Korea University, Seoul, Republic of Korea

<sup>g</sup>School of Electrical and Electronic Engineering, Yonsei University, Seoul, Republic of Korea

†Electronic supplementary information (ESI) available. See DOI: 10.1039/d0bm00847h

‡These authors contributed equally to this work.

ibility, biodegradability, porosity, and capacity of the sprouting axonal guidance.<sup>5</sup> The material used for its preparation is a major factor affecting the quality of the NGC. Synthetic polymer-based nerve scaffolds are gaining attention owing to their stable long-term performance in comparison with natural products. Among these materials, poly(lactide-*co*-caprolactone) (PLCL) has been investigated as a biomaterial suitable for tissue engineering, such as wound healing,<sup>6</sup> formation of cartilage<sup>7</sup> and cardiovascular<sup>8</sup> applications owing to its biocompatible and biodegradable nature and favorable mechanical properties, specifically high elasticity and flexibility. The suitability of PLCL for NGCs has already been proved by the current commercially available FDA-approved nerve conduits such as Neurolac®.<sup>2,5,9</sup>

During peripheral nerve regeneration following injury, Schwann cells play a significant role in three distinct manners: proliferation, development of bands of Bungner, and secretion of adequate growth factors.<sup>10</sup> However, Schwann cells with longer gaps are incapable of migrating and aligning through the gap, necessitating the use of topographical guidance structures for axonal sprouting.<sup>11,12</sup> To provide a suitable environment inside the conduit for axonal growth, several approaches have focused on filling the lumen with various shapes, such as hydrogel filling, micro/nanofilament filling, and micro/nano groove patterns.<sup>10</sup> On the one hand, a hollow lumen has the benefit of permitting sufficient space for free nerve regeneration, inducing axons to regrow to their suitable distal target. On the other hand, a lumen containing any type of luminal structure can have a mechanical or biological role that favors cell ingrowth, guidance, and correct targeting. For example, addition of growth factors or cells, and creation of unidirectional cryogel or microtube arrays in NGCs have demonstrated the achievement of directional axon growth, mimicking native autografts.<sup>13–15</sup>

Thus, the design of the interior of the NGC is expected to be a crucial factor to achieve effective axon regeneration across the gap.

Herein, we have developed NGCs based on PLCL membranes combined with 3D printed collagen hydrogel. PLCL membranes were obtained by electrospinning, which is a versatile technique for achieving micro to nanoscale topography and high porosity similar to the natural extracellular matrix. Porous PLCL membranes were fabricated with selective permeability to prevent fibrous tissue invasion but allow permeation of nutrients/oxygen.<sup>16</sup> The collagen hydrogel was utilized as a bioink for 3D printing to fill the PLCL conduit.

Although numerous previous studies have reported 3D printing with collagen-based bioinks, most of them used collagen blend or chemically modified-collagen owing to the difficulty in the printing of native unmodified collagen.<sup>17,18</sup> The extrusion 3D bioprinting of collagen requires a higher concentration, which achieves a viscosity suitable for extrusion.<sup>19</sup> However, the resolution is low in this method because the acidic collagen solution is diluted by neutralization with sodium hydroxide solution.<sup>20,21</sup> Recently, high-resolution 3D

bioprinting of collagen has been reported, which introduced a supporting bath composed of a gelatin microparticle slurry.<sup>22</sup> However, native collagen 3D printing without a supporting bath or sacrificial scaffold has not been reported yet.

In this study, we successfully performed 3D printing of native unmodified collagen without a supporting bath by using a dense collagen solution. Formation of fibrillar collagen gels by pH neutralization of acidic collagen solutions with ammonia vapor diffusion assisted in shape retention of the 3D printed collagen.<sup>23–26</sup> We believe that the concept of the fabrication of NGCs by integrating the 3D printed collagen hydrogel and electrospun PLCL membrane will provide promising modality in the field of NGCs. Finally, we compared the efficacies of PLCL conduits filled with bulk collagen and 3D printed collagen with the autogenous nerve graft for peripheral nerve regeneration, and proved the advantages of NGCs with a 3D printed collagen hydrogel based on the axonal growth, remyelination, and functional recovery.

## 2. Materials and methods

### 2.1 Preparation of PLCL membranes

PLCL (LA:CL = 50:50) was synthesized as previously reported.<sup>27,28</sup> PLCL with average number of molecular weight  $128\,000 \pm 15\,000 \text{ g mol}^{-1}$  was dissolved in HFIP (1,1,1,3,3,3-hexafluoroisopropanol, TCI, Japan) at 5% (w/v) concentration. A syringe was loaded with 12 ml of the solution and placed on a syringe pump. An electric potential was applied to the metallic needle (19 G) *via* the high-voltage power supply. The applied voltage was 21 kV, the solution flow rate was  $0.4 \text{ ml h}^{-1}$ , and the distance between the tip of the needle and the drum collector was 12 cm. The diameter of the drum collector was 8 cm and the rotation speed of the drum was 300 rpm.

### 2.2 Bioink preparation and 3D printing of the collagen hydrogel

Highly concentrated collagen solution was obtained by setting collagen solutions into Amicon® (Sigma Aldrich, USA) centrifugal devices (3 kDa cut-off) and centrifuging until the desired concentration was reached. For the 3D printing bioink, acidified type I collagen (Corning, USA) was adjusted to a final concentration of  $22 \text{ mg ml}^{-1}$ . Then, the bioink was transferred to a 10 ml (12 ml) NORM-JECT® Luer Lock syringe with a Nordson EFD SmoothFlow™ tapered tip (0.2 mm). The syringe was placed in a bio dispenser (Rokit Invivo, ROKIT Inc., Korea) and 2 rectangular layers with 8 mm and 4.7 mm widths were printed onto the electrospun PLCL membrane using NewCreatorK 3D printing software. The slicer setting was: 0.2 mm layer height, 40% fill density, single line pattern,  $10 \text{ mm s}^{-1}$  printing speed,  $10 \text{ mm s}^{-1}$  traveling speed, and 250% input flow. The viscosity of the collagen bioink was measured using a Brookfield RVDV-III viscometer (Brookfield, USA) under a fixed temperature of 25 °C.

Following 3D printing, short y-traversed deposition between each track of longitudinal collagen line was removed, since we assumed that it would hamper the ingrowth of neural cells along the conduits. After removing this, dense collagen line patterns were prepared by neutralization of the concentrated solutions in ammonia vapors.<sup>23–26</sup> 3D printed line patterns were exposed to ammonia vapor for 30 min and then removed from the chamber, followed by incubation at 37 °C for 10 min. Finally, the solidified gel was rinsed with 1× PBS buffer and immersed in PBS buffer for 1 h to remove excess ammonia.

### 2.3 Fabrication of the elastic nerve guidance conduit

A tubular nerve guidance conduit (NGC) with a patterned collagen hydrogel was fabricated by rolling the collagen-printed porous PLCL membrane (Fig. 1). The membrane was rolled into a tubular shape, and the end of the membrane was closed tightly using a medical adhesive (Adapt 7730, Hollister, USA). The medical adhesive was applied with a fine brush. The fabricated NGC had an inner diameter of 1.5–2.0 mm, a length of 10 mm, and a wall thickness (*i.e.*, thickness of PLCL membranes) of ~91 μm. For the fabrication of an NGC with the bulk collagen hydrogel as the control for the NGC with a 3D printed collagen hydrogel, the bare PLCL membrane was first rolled into a tubular shape and closed with a medical adhesive. Subsequently, acidified collagen was injected into the hollow tube and exposed to ammonia vapor, as in the procedure for the fabrication of NGCs with a 3D printed collagen hydrogel.

### 2.4 Characterization of the developed elastic nerve guidance conduit

The thickness and the average pore size of the PLCL membrane were measured using cross-section and topography of SEM images using Image J (National Institute of Mental

Health, USA). The diameter of the PLCL nanofiber was analyzed using image processing software, Diameter J (National Institutes of Mental Health, USA). For collagen hydrogel characterization, the samples were freeze-dried followed by SEM observation. The vacuum-dried PLCL membranes were gold-sputtered and their morphologies were characterized using a scanning electron microscope (SEM, Phenom Pro, Thermo Fisher, USA). Thickness of the 3D printed collagen hydrogel line and inter-gel spacing in freeze-dried and hydrated states are measured using Image J from SEM images and photographs.

### 2.5 *In vitro* cell study

PC12 cells (Korea Cell Line Bank, Korea; rat adrenal pheochromocytoma cell line) were cultured and grown in 75 cm<sup>2</sup> culture flasks in Roswell Park Memorial Institute (RPMI) medium supplemented with 10% horse serum and 1% penicillin–streptomycin (Gibco BRL) without the nerve growth factor at 37 °C in humid air with 5% (*v/v*) CO<sub>2</sub>. When the PC12 cells were grown to the logarithmic growth phase, they were seeded onto the PLCL membranes at the density of 10<sup>3</sup> or 10<sup>4</sup> cells per cm<sup>2</sup> and cultured.

To evaluate cell viability, PLCL membranes seeded with 10<sup>4</sup> cells per cm<sup>2</sup> were tested using a live/dead viability kit. The cell-laden membranes were washed with PBS and immersed in an aqueous solution containing 2 μM calcein AM (Thermo Fisher, USA) and 4 μM ethidium homodimer-1 (Thermo Fisher, USA) for 30 min at 37 °C. Subsequently, fluorescence images were acquired using a confocal laser scanning microscope (CLSM, LSM700, Zeiss, Germany). Immunofluorescence staining was performed to confirm the neurogenic differentiation of PC12 cells on the membranes. One week after the cell culture at a density of 10<sup>3</sup> cells per cm<sup>2</sup>, the membranes with the seeded cells were fixed and stained with the β-tubulin

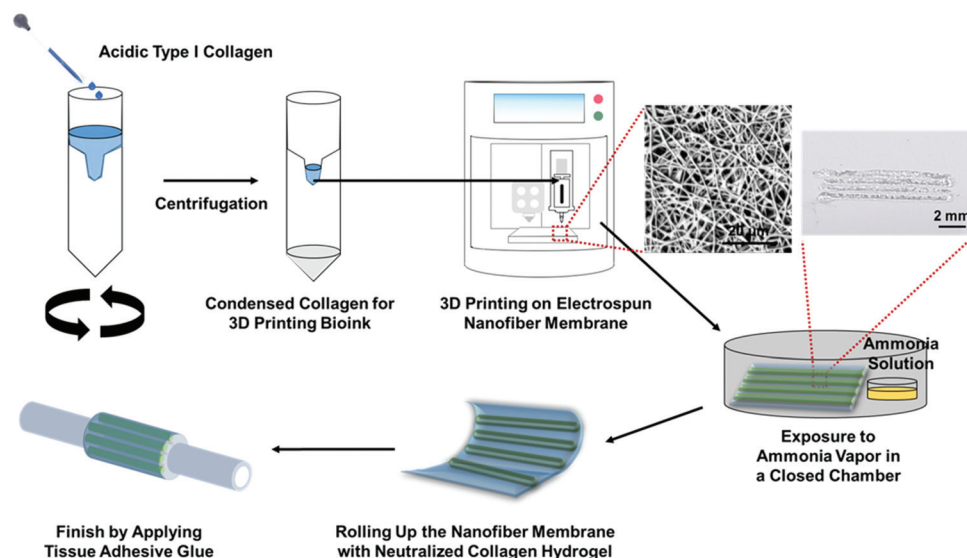


Fig. 1 Schematic illustration of the fabrication of nerve guidance conduits with the 3D printed collagen hydrogel.

III antibody (T8578, Sigma, USA). Alexa 488 anti-mouse IgG (Abcam, UK) was used as a secondary antibody, and the nuclei were counterstained with DAPI (Molecular Probes, USA). Subsequently, the stained samples were observed using a CLSM. The immunofluorescence staining images of the PC12 cells were analyzed using Image J. The ratio of neurite-bearing cells was calculated by counting the number of differentiated cells and the total number of cells in randomly selected areas. Only PC12 cells longer than or equal to the diameter of the cell body were considered to be differentiated.<sup>29–31</sup>

## 2.6 Experimental animals and surgical procedures

All animal experiments were conducted on male Lewis rats weighing 250 to 300 g in accordance with the recommendations contained in the Guideline of Association for Assessment and Accreditation of Laboratory Animal Care International (AAALAC International) and approved by the Institutional Animal Care and Use Committee of the Korea University College of Medicine (IACUC Approval no. 2018-0138). The animals were randomly divided into three experimental groups: nerve autograft (Autograft group,  $n = 10$ ), NGC occupied by the bulk collagen hydrogel (Bulk group,  $n = 10$ ) and NGC occupied by a 3D printed collagen hydrogel (3D printing group,  $n = 12$ ). For performing the surgery, the animals were anesthetized by inhalation of isoflurane and the left sciatic nerve of each animal was exposed at the mid-thigh level from the inferior margin of the piriformis muscle approximately 5 mm distal to the bifurcation. An 8 mm-long segment of the sciatic nerve was excised with sharp microsurgical scissors under an operating microscope. In animals in the Autograft group, the excised nerve segment between proximal and distal stumps was reversed and repaired using five 10–0 epineurial interrupted sutures (Ethilon®, Ethicon Inc., Somerville) at each end of the stump. For the Bulk collagen and 3D printing groups, each 12 mm sized NGC filled with the bulk collagen hydrogel or the 3D printed collagen hydrogel was inserted between proximal and distal stumps using five 10–0 epineurial interrupted sutures at each stump, while the ends of each stump were inserted 2 mm into the conduit sleeve to create a uniform 8 mm nerve defect. Finally, the skin was closed with 4–0 interrupted sutures (Ethilon®). The right (contralateral) sciatic nerve was left intact and served as an intra-individual control. All animals were housed in groups of three animals in a temperature- and humidity-controlled environment with a 12-hour light/dark cycle and *ad libitum* access to food and water. The first postoperative functional testing was started after three weeks. During a total of 12 weeks of observation period, nonsurvival measurements including maximum isometric tetanic force, muscle weight ratio, and nerve histological evaluation were performed at two-time points, 6 weeks and 12 weeks. At 6 weeks, 4 animals from the Autograft group, 4 animals from the Bulk group and 5 animals from the 3D printing group were measured and sacrificed. At 12 weeks, all remaining animals (6, 6, and 7 animals, respectively) were measured. Survival measurements including

video gait analysis and ankle angle were measured every 3 weeks for live animals at each time point.

## 2.7 Assessment of the functional motor recovery

**2.7.1 Video gait analysis and ankle angle.** In order to assess the serial functional recovery after surgery, we measured the active ankle angle at terminal stance (ATS) every three weeks up to twelve weeks, as the angle in the gait cycle has been shown to the most well correlated with functional recovery.<sup>32,33</sup> At 3 and 6 weeks, all animals from each group were subjected to measurements, and at 9 and 12 weeks, 6 animals from the Autograft group, 6 animals from the Bulk group, and 7 animals from the 3D printing group. To obtain the animal gait video, a 20 cm-high transparent Plexiglas 48 cm long and 10 cm wide was attached on both sides of the walking treadmill. The treadmill was gradually accelerated to 20 cm s<sup>-1</sup> to allow the animal to walk straight in the forward direction, and images were acquired with a 60 Hz digital camera positioned at a distance of 1 m. The recordings were repeated until three satisfactory trials per animal were obtained. The frame of the video at the toe-off, *i.e.*, the moment of maximal plantar flexion of the experimental side ankle joint, was selected and the leg segment and the foot segment were manually identified for the terminal stance phase. The angle between the longitudinal axes of the tibia and foot segment was measured from still images using Image J. After the video gait analysis, the ankle contracture angle was determined by measuring the maximal passive plantarflexion angle, as previously described.<sup>34</sup> This was measured bilaterally using a transparent goniometer under deep sedation induced by isoflurane inhalation and recorded as a percentage of the contralateral side. Rats developed ankle contracture limiting plantar flexion at the resting position of the rats that keeps the ankles in dorsiflexion. A larger angle indicates less ankle contracture and therefore better motor functional recovery.

**2.7.2 Maximum isometric tetanic force.** The maximum isometric tetanic force of the tibialis anterior (TA) muscle was measured to evaluate reproducible quantitative motor recovery. Four animals of the Autograft group and Bulk group, and five animals of the 3D printing group were measured at six weeks to observe their midpoint functional recovery. The remaining animals were measured at twelve weeks using the previously described method (Fig. S1†).<sup>35</sup> In brief, the rats were anesthetized as before, and the TA tendon insertion site was exposed and released from the extensor retinaculum. The hind limb was stabilized on a wooden platform by two 0.035-inch Kirschner wires placed at the distal femur and distal tibia. The exposed tendon was tied with black silk thread, and the other end of the black silk thread was connected to an isometric force transducer (Harvard Apparatus, Holliston, MA). The signal was processed on a computer using Labscribe software (Iworx/CB Sciences, Dover, NH). Two small, custom-made hook-shaped bipolar stimulating electrodes using a CK-100 field stimulator (CB Science) were placed at the sciatic nerve proximal to the graft site. Equal stimulation pulses were applied to all the measurements: preload, 10 g; stimulus inten-



sity, 10 V; pulse duration, 2 ms; and pulse frequency, 100 Hz. The stimulations were applied five times and the TA muscle was rested for two minutes between the stimulations with no preload to avoid muscle fatigue. The highest force was determined as the maximum isometric tetanic force. The same procedure was performed on the contralateral side.

**2.7.3 Muscle weight ratio.** The animals were sacrificed after completion of the muscle tetanic force measurement. Owing to peripheral nerve injury, the muscle was denervated, which led to the tendency of muscle atrophy. The muscle was dissected carefully from the surrounding tissues and weighed in grams. The same evaluations were performed for the contralateral normal side and the weight was normalized using data of the contralateral side and reported as a percentage of the normal contralateral side (Fig. S1†).

## 2.8 Immunohistochemical evaluation

After harvesting the TA muscle, the regenerated nerve tissues with the surrounding NGC or autograft were also harvested to investigate the nerve fiber growth through the NGCs. Specimen from 1 animal of the Autograft and Bulk collagen group and 2 animals of the 3D printing group at 12 weeks were fixed and then immersed in cryoembedding media (Tissue-Tek® O. C. T. Compound, Sakura Finetechnical Co., Japan) and frozen immediately at  $-80\text{ }^{\circ}\text{C}$ , following which they were cut into longitudinal sections of  $10\text{ }\mu\text{m}$  thickness. Microtubule protein  $\beta$ -tubulin III and S100 were used as specific markers for neurons and Schwann cells, respectively. The sectioned specimens were incubated overnight at room temperature for primary antibodies ( $\beta$ -tubulin III (T8578, Sigma, USA), S100 (ab52642, Abcam, UK), followed by incubation in Alexa 488 anti-mouse IgG (Abcam, UK) and Alexa 594 anti-rabbit IgG (Abcam, UK). The nuclei were counterstained with DAPI (Molecular Probes, USA), and the stained sections were observed by CLSM.

## 2.9 Nerve histomorphometric analysis

Along with the harvesting of the regenerated nerve tissue and nerve conduits for nerve histology, distal nerve segments (5 mm segments harvested 1 mm distal to the distal suture) were harvested to investigate peripheral nerve regeneration through the NGCs. The nerve specimens were fixed with 2.5% glutaraldehyde in  $0.1\text{ mol L}^{-1}$  phosphate buffer (pH 7.4) for 48 h at room temperature and post-fixed with 1% osmium tetroxide. The nerve specimens were embedded in epoxy resin, cut into  $1\text{ }\mu\text{m}$ , semi-thin sections with an ultramicrotome, and stained with 1% toluidine blue for light microscopy (BX46, Olympus, Japan). The images were digitized with a charge-coupled device camera (DP21, Olympus, Japan) and analyzed using standard image processing at a magnification of  $\times 20$ . The tibial nerve cross-section was analyzed using ImageJ software (Fiji Distribution, National Institute of Health, Bethesda, MA). The total number of axons, cross-sectional area, myelinated fiber area, N ratio, G ratio and mean axon density were determined for specimens obtained at 12 weeks from 4 animals from the Autograft group, 4 animals from the Bulk

group, and 5 animals from the 3D printing group. The myelin thickness and G ratio, calculated as the axon diameter divided by total fiber diameter, were measured at  $\times 60$  magnification, and averaged from five views obtained by random sampling. The N ratio, calculated as the total myelinated fiber area divided by the total tissue cable area, represents the information regarding the number of sprouting events.<sup>23</sup>

## 2.10 Statistical analysis

The statistical analysis was performed using one-way and two-way analysis of variance (ANOVA). The data are presented as mean  $\pm$  SD, and the Kolmogorov–Smirnov test was performed to determine the normality of the distributions. The Kruskal–Wallis test, with the *post hoc* Mann–Whitney test, was used to detect differences in the functional and histomorphometric parameters between the groups. All statistical analyses were performed using SPSS software (version 20, IBM, NY) and a value of  $p < 0.05$  was considered as statistically significant.

# 3. Results and discussion

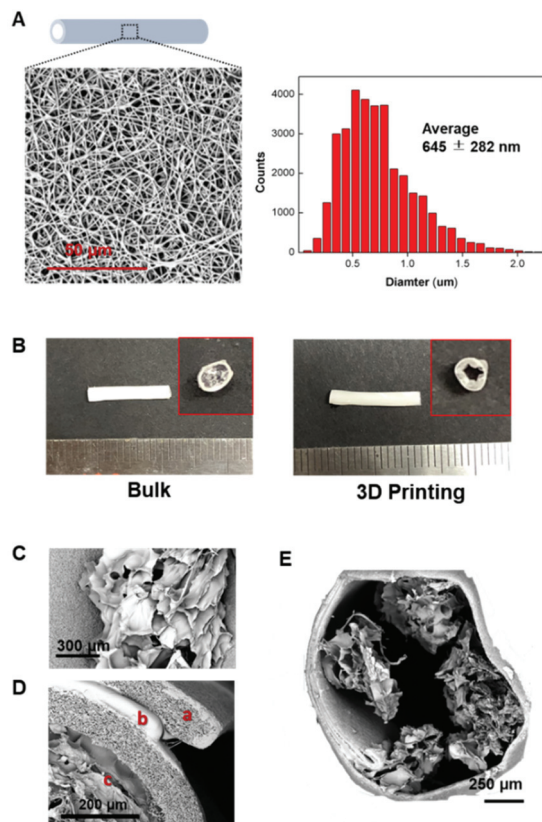
## 3.1 NGCs based on a porous PLCL membrane with a 3D printed collagen hydrogel

Fig. 1 illustrates the procedure for the fabrication of NGCs based on a porous PLCL membrane with a 3D printed collagen hydrogel. First, the concentrated collagen bioink was prepared *via* centrifugation using Amicon®, as explained in the Experimental section. A dense acidified collagen solution enables 3D printing without collapse of shape (Video S1†). The viscosity of the collagen bioink at  $2\text{ s}^{-1}$  shear rate was  $1.3 \times 10^5\text{ mPa s}$ , which is within the range of viscosity suitable for extrusion-based 3D printing according to the previous study.<sup>19</sup> A bioink suitable for extrusion 3D printing should have a high dynamic viscosity (from 30 to  $6 \times 10^7\text{ mPa s}$ ).

We printed the collagen bioink onto the PLCL porous membrane, which is made by electrospinning with an optimized pore size ( $2.7 \pm 0.6\text{ }\mu\text{m}$ ) to allow exchange of nutrients and oxygen but prevent cell penetration.<sup>16</sup> According to previous studies, infiltration of non-neural cells into the conduit lumen can occur when the wall pores are larger than  $10\text{ }\mu\text{m}$ .<sup>36,37</sup> Following 3D printing of the collagen hydrogel, the neutralization of acidified collagen was conducted by exposure to ammonia vapor to induce fibrillar collagen gel. Neutralization using vapor assists in maintaining the shape of the collagen hydrogel without crumbling. Subsequently, the collagen hydrogel was rinsed with PBS buffer to remove toxic residues in the hydrogel. The NGCs were finally prepared by rolling into a tubular shape and closed by applying a medical adhesive. The prepared NGCs were implanted in the rat sciatic nerve model.

## 3.2 Characterization of fabricated NGCs

The electrospun PLCL membrane was characterized using a scanning electron microscope (SEM). To prevent the penetration of cells into the NGCs, we reduced the size of the pore by extracting nano-sized fibers. The diameter of the nanofibers



**Fig. 2** Characterization of the fabricated NGCs. (A) SEM images of PLCL membranes and the average diameter of nanofibers measured using Diameter J. (B) Photographs of NGCs with the bulk collagen hydrogel and 3D printing hydrogel in the hydrated state. (C–E) SEM images.

was measured using Diameter J plugin based on the Image J analysis program (Fig. 2A).<sup>38</sup> Fig. 2B and Fig. S2† show photographs of collagen hydrogels in the hydrated state. Fig. S2(B)† displays the longitudinal cross-section of the NGCs, which demonstrates the consistency of the gel deposition along the length. Owing to the elastic properties of PLCL, the cross-sectioned PLCL curled when it was cut. In Fig. 2B, NGCs filled fully with the collagen hydrogel, *i.e.*, bulk collagen NGCs, show no empty space. In contrast, NGCs with a 3D printed collagen hydrogel have an empty space even in the hydrated state. The conduit fill ratio calculated based on the hydrated cross-sectional photographs is  $72 \pm 2\%$ . We compared the bulk and 3D printed collagen hydrogel NGCs to clarify the effect of 3D printing by excluding the effect of the material, collagen hydrogel, for nerve regeneration. Fig. 2C–E show SEM images following freeze-drying. The 3D printed collagen hydrogel has approximately 500 μm of resolution in the hydrated state (Fig. 2C and Fig. S3†). We conjectured that the thickness of the collagen line slightly decreased in the dried state compared with the hydrated state due to the high concentration of collagen solution. The porous PLCL membrane, medical adhesive, and collagen hydrogel were observed by SEM (Fig. 2D). Furthermore, we confirmed that collagen line pat-

terns remained intact even when the membranes were rolled up, proving the solidification of the collagen hydrogel (Fig. 2E).

### 3.3 Cell behaviors on the PLCL membrane and membrane with a 3D printed collagen hydrogel

To investigate the biocompatibility of the PLCL membrane and collagen hydrogel, PC12 cells were cultured on the PLCL membrane and the PLCL membrane with the 3D printed collagen hydrogel. The viability on each surface was measured by live/dead assay after 5 days. The data indicate that the PC12 cells endured the 5-day period and there was little difference between the two surfaces. This indicates that the PLCL membrane and collagen hydrogel are biocompatible and do not demonstrate the effects of acid and base conditions used during the gelation process of collagen (Fig. S4†). Next, the PC12 cells were cultured on each surface for 1 week and then the cytoplasm ( $\beta$ -tubulin III) and nucleus of the PC12 cells were stained for neurite differentiation analysis. The differentiated PC12 cells were rarely found on PLCL membranes, and the cells were relatively round in shape. However, the differentiation of PC12 cells into neuron-like elongated cells was observed on the surfaces of the 3D printed collagen; the extended axons are marked with white arrows in Fig. 3. The percentages of differentiated cells on collagen grafted PLCL membranes were relatively lower than previous studies since we excluded the treatment of nerve growth factor,<sup>31,39</sup> but significantly higher compared to bare PLCL membranes. Thus, we have confirmed that the line pattern of collagen hydrogel induced increased cell adhesion and promoted cell differentiation.

### 3.4 Functional motor recovery evaluation

**3.4.1 General observation following surgery and weight gain.** All animals showed a progressive gain in weight and mobility after surgical procedure. At twelve weeks, the mean percentage of animal weight compared with the surgical procedure for the Autograft group I was  $124.9 \pm 1.8\%$ , and it was  $124.7 \pm 3.5\%$  for the Bulk group, and  $120.1 \pm 4.8\%$  for the 3D printing group. Significant differences between the groups were not found ( $p > 0.05$ ). None of the animals showed infection, delayed wound healing, or signs of auto-mutilation

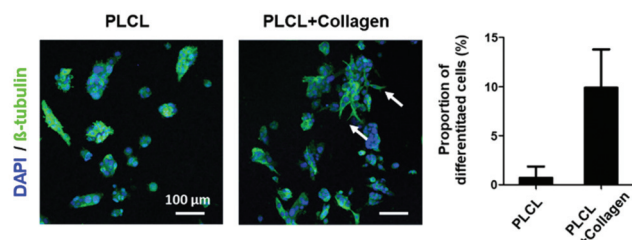


**Fig. 3** Immunofluorescence images and quantitative analysis of differentiated cells after 1 week of PC12 cell culture on PLCL membranes and PLCL membranes with the 3D printed collagen hydrogel. White arrows indicate neuron-like cells with extended axons.

throughout the study. Macroscopic signs of graft disconnection, or serous or neuroma formation were absent.

**3.4.2 Ankle angle measurements.** Fig. 4 summarizes the ankle contracture angles and ATS for the three animal groups measured every three weeks. The ankle contracture angles were significantly reduced until six weeks, and then gradually improved up to twelve weeks in all groups. At twelve weeks, the ankle contracture angles of the 3D printing group were similar to those of the Autograft group ( $89.68 \pm 2.37\%$  vs.  $93.52 \pm 3.17\%$  respectively,  $p > 0.05$ ). They were significantly higher than those of the Bulk group ( $83.86 \pm 4.64\%$ ,  $p < 0.05$ ). This pattern of recovery was also found in the ATS measurements, which deteriorated until six weeks to reach similar degrees. Interestingly, after six weeks, the Autograft and 3D printing groups gradually regained the ATS, whereas the Bulk group showed a decrease in the ATS over time. Twelve weeks after nerve reconstruction, both the Autograft and the 3D printing groups showed significantly higher ATS in comparison with the Bulk group ( $24.02 \pm 1.26^\circ$  vs.  $19.65 \pm 4.78^\circ$  vs.  $11.35 \pm 2.91^\circ$ , respectively,  $p < 0.05$ ). The Autograft group did not show statistical difference in ATS in comparison with the 3D printing group ( $p > 0.05$ ). These results indicate that the 3D printed line pattern of the collagen hydrogel encourages motor regeneration through the NGC, close to the gold standard reconstruction method. A sciatic functional index was not used in this study because of possible interference in its determination by toe contractures.

**3.4.3 Evaluations of the isometric tetanic force and muscle weight ratio.** The maximum isometric tetanic force measurements of TA muscles at six weeks after nerve reconstruction demonstrated significantly lower tetanic force in both the Bulk group and 3D printing group than in the Autograft group ( $10.64 \pm 12.90\%$  vs.  $16.33 \pm 7.39\%$  vs.  $49.79 \pm 13.53\%$  respectively,  $p < 0.05$ ). However, at the final examination at twelve

weeks, the 3D printing group reached a level comparable to that in the autologous nerve grafted animals, as shown in Fig. 5 ( $60.5 \pm 21.64\%$  vs.  $67.35 \pm 6.60\%$  respectively,  $p > 0.05$ ). In contrast, the Bulk group still showed significantly lower tetanic force compared with the Autograft group ( $39.87 \pm 21.27\%$  vs.  $67.35 \pm 6.60\%$ ,  $p < 0.05$ ).

As an additional indicator for motor recovery, the TA muscle wet weight ratios were determined. As depicted in Fig. 5, muscle atrophy in both the Bulk and 3D printing group

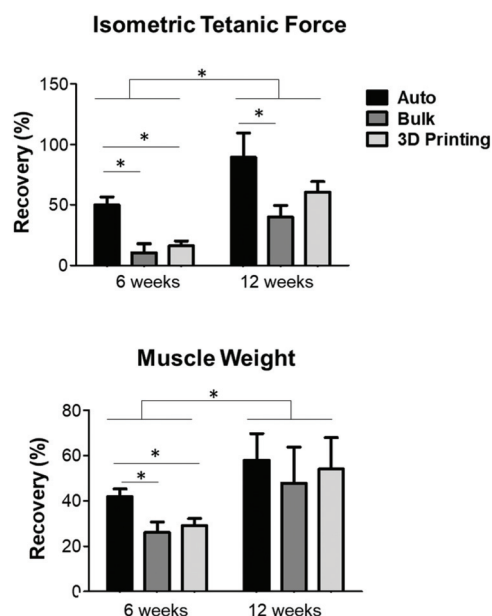


Fig. 5 The results of maximum isometric tetanic force and muscle weight ratio of tibialis anterior muscle measured at 6 and 12 weeks following nerve reconstruction. Data are presented as the percentage of the normal contralateral side. \* $p < 0.05$ .

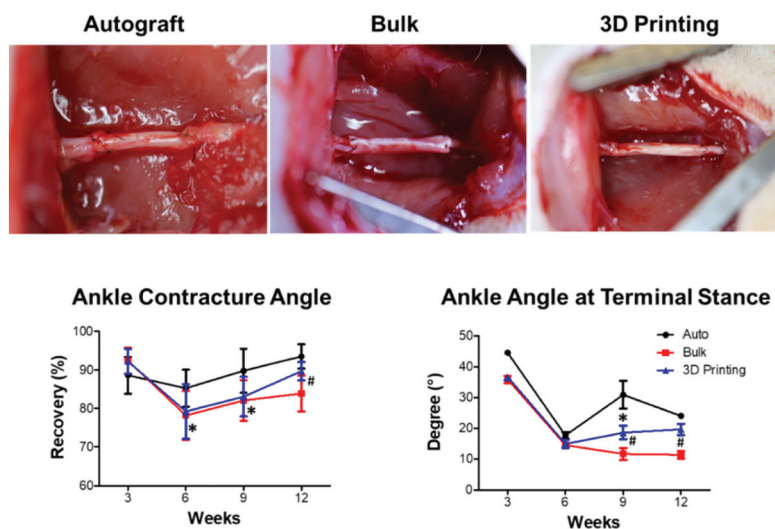


Fig. 4 Results of passive ankle contracture angle and active ankle angle at the terminal stance of all animal groups (Autograft, Bulk, and 3D printing groups) measured at 3, 6, 9, and 12 weeks following nerve reconstruction. \* $p < 0.05$  Autograft versus 3D printing group; # $p < 0.05$  Bulk group versus 3D printing group.



was significantly more severe than that in the Autograft group at six weeks ( $26.07 \pm 4.55\%$  vs.  $26.4 \pm 1.46\%$  vs.  $41.82 \pm 3.40\%$  respectively  $p < 0.05$ ). However, the Bulk and 3D printing groups recovered to a level closer to that of the Autograft group at twelve weeks ( $47.76 \pm 15.98\%$  vs.  $54.05 \pm 12.46\%$  vs.  $57.95 \pm 11.73\%$  respectively,  $p > 0.05$ ). Furthermore, the 3D printing group showed constantly higher ratios at both six weeks and twelve weeks without statistical significance. These results prove that the NGCs used in this study can promote nerve defect regeneration. The isometric tetanic force evaluation and the results of the ankle angles underscore the relatively high performance of the 3D printed collagen hydrogel.

### 3.5 Nerve regeneration through NGCs

Fig. 6 shows nerve regeneration with 8 mm defect size through the longitudinal direction in the NGCs at 12 weeks after surgery. The S100,  $\beta$ -tubulin, and DAPI mark Schwann cells, neurons, and cell nuclei, respectively. All groups demonstrated nerve regeneration along the NGCs, showing linear neuron penetration ( $\beta$ -tubulin) and Schwann cell (S100) integration into NGCs.<sup>40</sup> The Autograft group, as the positive group, showed a higher density of regenerated nerves than the other groups, as we expected. The NGCs with the 3D printed collagen hydrogel demonstrated linear guidance from the proximal to distal ends in comparison with the NGCs with bulk collagen.

Furthermore, an empty area, marked by white arrowheads, was observed in the Bulk collagen group, proving that its nerve regeneration ability was inferior to that of the 3D printing group. Fully filled collagen hydrogel in NGCs visibly reduced axonal regeneration, physically blocking the regenerated nerves.<sup>41</sup>

Nerve histology and morphometric analysis also supported the nerve regeneration through NGCs. To reveal regenerated tissue cable passing through each NGC, toluidine-blue stained single cross-sections were prepared at the mid-graft level of each group at six weeks. As shown in Fig. 7, all samples appeared to be connected through the NGCs with some regenerated endoneurial vessels being observed. As we intended, the tissue cables being regenerated were well retained in the PLCL membranes. The 3D printing collagen hydrogel showed a denser and organized pattern of regenerated axons, which was not observed in the case of bulk collagen. Morphometric analyses were performed on the nerve sections distal to the repair sites at twelve weeks to compare the morphologies of the regenerated axons and the surrounding myelin (Fig. 8A and Fig. S4†). The results, including the myelinated axon count, myelin fiber area, nerve fiber density, G ratio, N ratio, and myelin thickness measurements, of all animal groups are shown in Fig. 8B. Higher myelinated axon count and myelin thickness were found in the 3D printing group than in the

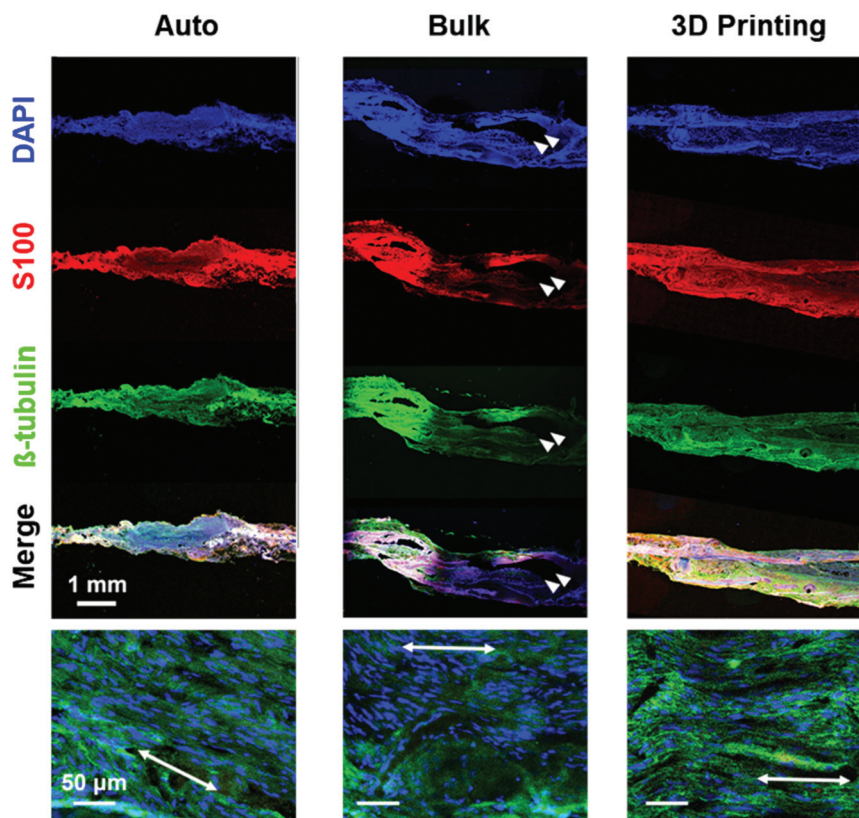


**Fig. 6** Longitudinal sections of the regenerated nerve through NGCs and autograft. Linear axon penetration and Schwann cell integration along with the NGCs. Neurons are labeled in green and Schwann cells in red. The white arrowheads indicate the empty area, proving the blocked regrowth of neurons. The double-headed arrows in magnified images in the bottom row indicate alignment direction of the regenerated nerves.



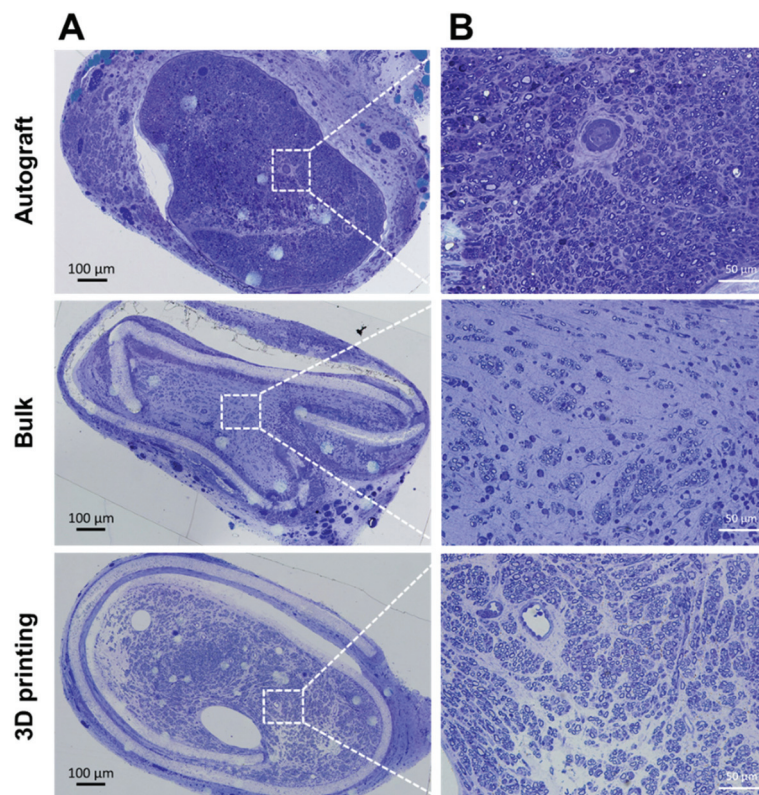


**Fig. 7** Histologic results of the mid-graft cross-section for all groups, 6 weeks after nerve reconstruction. (A) Regenerated axons were bridged inside the rolled porous PLCL membranes as well as in the Autograft (toluidine blue,  $\times 10$ ). (B) The random areas in the sample of each group were imaged at  $\times 40$  magnification. The myelinated axons were denser and organized in the Autograft group and 3D printing group in comparison with the Bulk group.

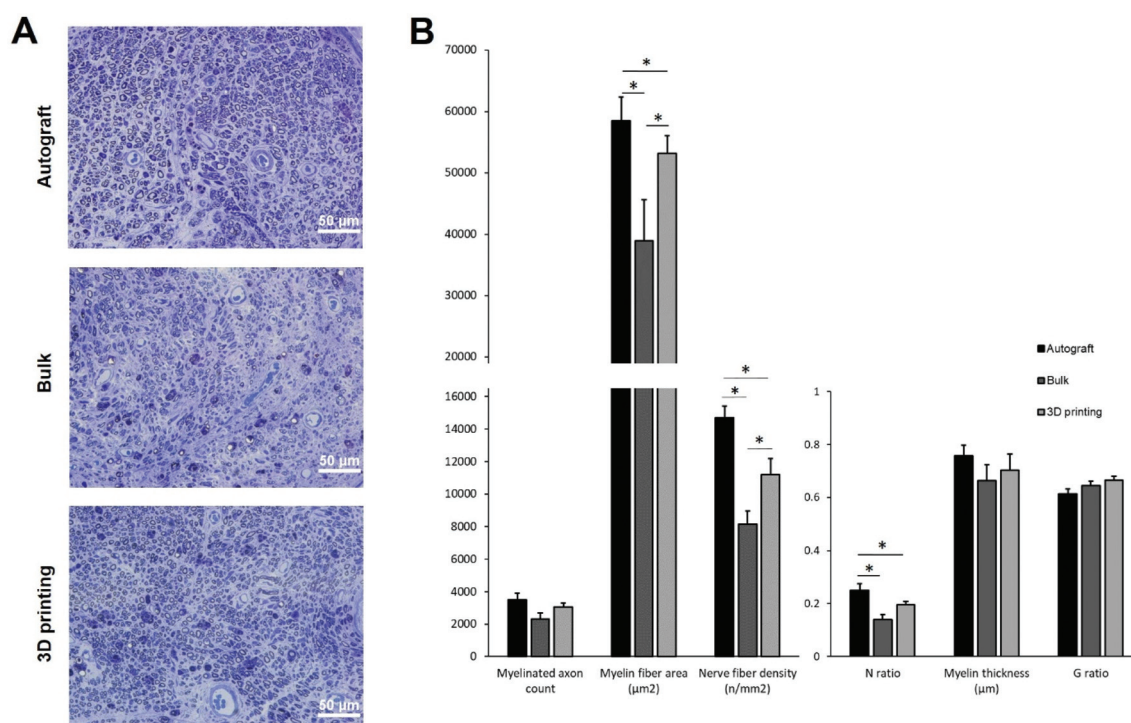


**Fig. 8** (A) Representative histological cross-sections obtained from distal to the graft at 12 weeks (toluidine blue,  $\times 40$ ). (B) The distal nerve (5 mm segment harvested 1 mm distal to the distal suture) was morphometrically analyzed in order to assess the myelinated fibers. Results of the myelinated axon count, myelin fiber area, nerve fiber density, N ratio, myelin thickness, and G ratio measurements were compared between groups.  $*p < 0.05$ .

Bulk group without statistical differences between the groups ( $p > 0.05$  for all). With regard to myelin fiber area and nerve fiber density, both the Bulk and 3D printing groups differed from the Autograft group (myelin fiber area,  $38\,928 \pm 13\,252 \mu\text{m}^2$  vs.  $53\,134 \pm 5893 \mu\text{m}^2$  vs.  $58\,481 \pm 6707 \mu\text{m}^2$  respectively,  $p < 0.05$ ; nerve fiber density,  $8153 \pm 1606 \text{ n mm}^{-2}$  vs.  $11\,206 \pm 1980 \text{ n mm}^{-2}$  vs.  $14\,702 \pm 1264 \text{ n mm}^{-2}$ ,  $p < 0.05$ ), and the 3D printing group showed higher values than the Bulk collagen group ( $p < 0.05$ ). The G ratio was found similar among the groups (Autograft group:  $0.67 \pm 0.06$ , Bulk group:  $0.61 \pm 0.08$ , 3D printing group:  $0.64 \pm 0.08$ ,  $p > 0.05$ ). The N ratio was significantly different in all groups ( $0.249 \pm 0.041$  vs.  $0.136 \pm 0.038$  vs.  $0.195 \pm 0.028$  respectively,  $p < 0.05$ ), but it was significantly lower in the Bulk collagen group in comparison with the Autograft group ( $p < 0.05$ ). The NGCs with various designs and materials have been experimentally examined for the reconstruction of peripheral nerve defects.<sup>42</sup> Although NGCs used in this experiment do not contain any growth factors or bioactive molecules, we found that the quality of axonal regeneration could be promoted by the 3D printed collagen hydrogel in the NGC. Intraluminal aligned patterning of collagen can serve as a guide for axonal growth in the conduit during the nerve regeneration period, as also demonstrated by the longitudinal histologic section. This finding was in line with the previously reported *in vitro* study using a 3D printed fibrin hydrogel.<sup>43</sup> The aligned hydrogel can provide additional haptotactic cues for Schwann cell growth as well as the directional micro-guidance for regenerated axons. The technique presented here enables this alignment without the need for complex processing of microchannel fabrication. It was found that when used over a porous PLCL structure, axons along the aligned hydrogel seem to be well protected and preserved *in vivo* while growing across the whole nerve defect. Future attempts should be made to determine ideal thickness and distance of 3D printed hydrogel alignment to optimize its guidance role. It should also be verified whether the collagen hydrogel in the NGCs can effectively deliver neuro-regenerative factors and bioactive molecules.

## 4. Conclusions

We developed NGCs with a 3D printed collagen hydrogel, which provided a guidance path along the longitudinal direction and ultimately promoted sciatic nerve regeneration. First, an acidified collagen bioink was 3D printed onto a PLCL porous membrane; then, neutralization was performed *via* ammonia vapor to maintain the 3D printed pattern. Following the solidification of the collagen hydrogel, the membrane was rolled into a tubular shape and fixed with medical adhesive. The crucial effect of 3D printing was demonstrated by comparing the NGCs with those filled with bulk collagen. We systematically confirmed the beneficial effects of NGCs with the 3D printed collagen hydrogel on axonal regeneration, remyelination, and functional recovery. Moreover, the 3D printed collagen hydrogel was prepared by simple centrifugation to

achieve a concentrated collagen bioink. Therefore, various types of growth factors or bioactive molecules can be easily incorporated in the collagen by simple centrifugation, which proves the vast potential of the method introduced in this study.

## Conflicts of interest

There are no conflicts to declare.

## Acknowledgements

This research was supported by the Exploratory Research Grant of the Korea University Medicine and Korea Institute of Science and Technology (2V08550 and K2010121) and the Nano-Material Technology Development Program (NRF2018M3A7B4071106) through the National Research Foundation of Korea funded by the Ministry of Science and ICT.

## References

- 1 F. Mohamadi, S. Ebrahimi-Barough, M. R. Nourani, A. Ahmadi and J. Ai, *Artif. Cells, Nanomed., Biotechnol.*, 2018, **46**, 34–45.
- 2 P. Chrzaszcz, K. Derbisz, K. Suszynski, J. Miodonski, R. Trybulski, J. Lewin-Kowalik and W. Marcol, *Neurol. Neurochir. Pol.*, 2018, **52**, 427–435.
- 3 A. R. Dixon, S. H. Jariwala, Z. Bilis, J. R. Loverde, P. F. Pasquina and L. M. Alvarez, *Biomaterials*, 2018, **186**, 44–63.
- 4 O. S. Manoukian, J. T. Baker, S. Rudraiah, M. R. Arul, A. T. Vella, A. J. Domb and S. G. Kumbar, *J. Controlled Release*, 2020, **317**, 78–95.
- 5 A. R. Nectow, K. G. Marra and D. L. Kaplan, *Tissue Eng., Part B*, 2012, **18**, 40–50.
- 6 T. H. Kim, Y. Jung and S. H. Kim, *Tissue Eng., Part A*, 2018, **24**, 830–848.
- 7 S. Lee, K. Lee, S. H. Kim and Y. Jung, *Polymers*, 2017, **9**, 348–363.
- 8 M. Shafiq, Y. Jung and S. H. Kim, *Eur. Cells Mater.*, 2015, **30**, 282–302.
- 9 A. L. Luis, J. M. Rodrigues, J. V. Lobato, M. A. Lopes, S. Amado, A. P. Veloso, P. A. S. Armada-da-Silva, S. Raimondo, S. Geuna, A. J. Ferreira, A. S. P. Varejao, J. D. Santos and A. C. Mauricio, *Bio-Med. Mater. Eng.*, 2007, **17**, 39–52.
- 10 C. R. Carvalho, J. M. Oliveira and R. L. Reis, *Front. Bioeng. Biotechnol.*, 2019, **7**, 337.
- 11 S. Houshyar, A. Bhattacharyya and R. Shanks, *ACS Chem. Neurosci.*, 2019, **10**, 3349–3365.
- 12 M. D. Sarker, S. Naghieh, A. D. McInnes, D. J. Schreyer and X. Chen, *Prog. Neurobiol.*, 2018, **171**, 125–150.
- 13 A. Singh, P. A. Shiekh, M. Das, J. Seppala and A. Kumar, *Biomacromolecules*, 2019, **20**, 662–673.

- 14 A. Singh, S. Asikainen, A. K. Teotia, P. A. Shiekh, E. Huutilainen, I. Qayoom, J. Partanen, J. Seppala and A. Kumar, *ACS Appl. Mater. Interfaces*, 2018, **10**, 43327–43342.
- 15 P. Labroo, D. Hilgart, B. Davis, C. Lambert, H. Sant, B. Gale, J. E. Shea and J. Agarwal, *Biotechnol. Bioeng.*, 2019, **116**, 143–154.
- 16 S. H. Oh, J. G. Kang, T. H. Kim, U. Namgung, K. S. Song, B. H. Jeon and J. H. Lee, *J. Biomed. Mater. Res., Part A*, 2018, **106**, 52–64.
- 17 N. Diamantides, L. Wang, T. Pruiksma, J. Siemiatkoski, C. Dugopolski, S. Shortkroff, S. Kennedy and L. J. Bonassar, *Biofabrication*, 2017, **9**, 034102.
- 18 H. Stratesteffen, M. Kopf, F. Kreimendahl, A. Blaeser, S. Jockenhoevel and H. Fischer, *Biofabrication*, 2017, **9**, 045002.
- 19 L. Valot, J. Martinez, A. Mehdi and G. Subra, *Chem. Soc. Rev.*, 2019, **48**, 4049–4086.
- 20 S. Rhee, J. L. Puetzer, B. N. Mason, C. A. Reinhart-King and L. J. Bonassar, *ACS Biomater. Sci. Eng.*, 2016, **2**, 1800–1805.
- 21 J. Y. Park, J. C. Choi, J. H. Shim, J. S. Lee, H. Park, S. W. Kim, J. Doh and D. W. Cho, *Biofabrication*, 2014, **6**, 035004.
- 22 A. Lee, A. R. Hudson, D. J. Shiwerski, J. W. Tashman, T. J. Hinton, S. Yernei, J. M. Bliley, P. G. Campbell and A. W. Feinberg, *Science*, 2019, **365**, 482–487.
- 23 C. Helary, L. Ovtracht, B. Coulomb, G. Godeau and M. M. Giraud-Guille, *Biomaterials*, 2006, **27**, 4443–4452.
- 24 S. Vigier, C. Catania, B. Baroukh, J. L. Saffar, M. M. Giraud-Guille and M. L. Colombier, *Tissue Eng., Part A*, 2011, **17**, 889–898.
- 25 A. Tidu, D. Ghoubay-Benallaoua, C. Teulon, S. Asnacios, K. Grieve, F. Portier, M. C. Schanne-Klein, V. Borderie and G. Mosser, *Biomater. Sci.*, 2018, **6**, 1492–1502.
- 26 J. Wang, Y. Qu, C. Chen, J. Sun, H. Pan, C. Shao, R. Tang and X. Gu, *Mater. Sci. Eng., C*, 2019, **104**, 109959.
- 27 S. I. Jeong, S. H. Kim, Y. H. Kim, Y. Jung, J. H. Kwon, B. S. Kim and Y. M. Lee, *J. Biomater. Sci., Polym. Ed.*, 2004, **15**, 645–660.
- 28 S. I. Jeong, B. S. Kim, S. W. Kang, J. H. Kwon, Y. M. Lee, S. H. Kim and Y. H. Kim, *Biomaterials*, 2004, **25**, 5939–5946.
- 29 Y. Liu, S. Yu, X. Gu, R. Cao and S. Cui, *J. Neural Eng.*, 2019, **16**, 036030.
- 30 Y. Yang, W. Zhao, J. He, Y. Zhao, F. Ding and X. Gu, *Eur. J. Pharm. Biopharm.*, 2011, **79**, 519–525.
- 31 G. B. Kim, Y. Chen, W. Kang, J. Guo, R. Payne, H. Li, Q. Wei, J. Baker, C. Dong, S. Zhang, P. K. Wong, E. B. Rizk, J. Yan and J. Yang, *Biomaterials*, 2018, **178**, 504–516.
- 32 P. Yu, H. S. Matloub, J. R. Sanger and P. Narini, *Muscle Nerve*, 2001, **24**, 231–239.
- 33 J. Y. Lee, G. Giusti, H. Wang, P. F. Friedrich, A. T. Bishop and A. Y. Shin, *Plast. Reconstr. Surg.*, 2013, **132**, 1173–1180.
- 34 J. P. Kim, C. A. Hundepool, P. F. Friedrich, S. L. Moran, A. T. Bishop and A. Y. Shin, *Microsurgery*, 2018, **38**, 66–75.
- 35 R. H. Shin, T. Vathana, G. A. Giessler, P. F. Friedrich, A. T. Bishop and A. Y. Shin, *Microsurgery*, 2008, **28**, 452–457.
- 36 E. B. Saltzman, J. C. Villa, S. B. Doty, J. H. Feinberg, S. K. Lee and S. W. Wolfe, *J. Hand Surg. Am.*, 2019, **44**, 700.
- 37 M. Ezra, J. Bushman, D. Shreiber, M. Schachner and J. Kohn, *Tissue Eng., Part A*, 2016, **22**, 818–826.
- 38 N. A. Hotaling, K. Bharti, H. Kriel and C. G. Simon Jr., *Biomaterials*, 2015, **61**, 327–338.
- 39 J. A. Sierra-Fonseca, O. Najera, J. Martinez-Jurado, E. M. Walker, A. Varela-Ramirez, A. M. Khan, M. Miranda, N. S. Lamango and S. Roychowdhury, *BMC Neurosci.*, 2014, **15**, 132.
- 40 D. Zhang, Y. Yao, Y. Duan, X. Yu, H. Shi, J. R. Nakkala, X. Zuo, L. Hong, Z. Mao and C. Gao, *ACS Appl. Mater. Interfaces*, 2020, **12**, 7915–7930.
- 41 C. Meyer, S. Wrobel, S. Raimondo, S. Rochkind, C. Heimann, A. Shahar, O. Ziv-Polat, S. Geuna, C. Grothe and K. Haastert-Talini, *Cell Transplant.*, 2016, **25**, 159–182.
- 42 X. Gu, F. Ding and D. F. Williams, *Biomaterials*, 2014, **35**, 6143–6156.
- 43 S. England, A. Rajaram, D. J. Schreyer and X. Chen, *Bioprinting*, 2017, **5**, 1–9.